The Validation of the Finite Difference Method and Reciprocity for Solving the Inverse Problem in EEG Dipole Source Analysis

Bart Vanrumste*+, Gert Van Hoey*+, Rik Van de Walle*, Michel R.P. D'Havé+, Ignace A. Lemahieu*, and Paul A.J.M. Boon+

Summary: The performance of the finite difference reciprocity method (FDRM) to solve the inverse problem in EEG dipole source analysis is investigated in the analytically solvable three-shell spherical head model for a large set of test dipoles. The location error for a grid with 2 mm and 3 mm node spacing is in general, not larger than twice the internode distance, hence 4 mm and 6 mm, respectively. Increasing the number of scalp electrodes from 27 to 44 only marginally improves the location error. The orientation error is always smaller than 4° for all the test dipoles considered. We have also compared the sensitivity to noise using FDRM in EEG dipole source analysis with the sensitivity to noise using the analytical expression for the forward problem. FDRM is not more sensitive to noise than the method using the analytical expression.

Key words: EEG dipole source analysis; Finite difference method; Reciprocity; Number of electrodes; Noise.

Introduction

An electroencephalogram (EEG) measures potential differences at scalp electrodes as a function of time. The generators of the EEG are a sufficient number of pyramidal cells located in the cortex which depolarize and repolarize (Schaul 1998) synchronously. In epilepsy (Boon and D'Havé 1995; Boon et al. 1996; Ebersole and Wade 1990) and evoked potentials (Lopes da Silva 1987) there is a need to localize the generators of the EEG. A source model often utilized is the current dipole, which represents a focal area of synchronously active pyramidal cells. The forward problem starts from a given dipole and calculates the potentials measured at the scalp electrodes. The inverse problem seeks the optimum dipole parameters for a given potential distribution at the scalp electrodes. This can be done by scanning through a fixed set of dipoles and choosing that dipole yielding potentials which best fit the measured EEG. Here a large number of forward calculations (corresponding with the fixed set of dipoles) need to be carried out prior to the inverse procedure. Another way to solve the inverse problem is by iteratively adjusting the dipole parameters. Here the forward evaluations are performed while solving the inverse problem. We apply this last method to solve the inverse problem. For both methods, the scanning and the iterative method, a large number (several hundreds) of forward evaluations must be carried out. As such, relatively fast forward evaluations are needed.

Numerical methods solve the forward problem in realistically shaped head models. The boundary-element method (BEM) (Meijs et al. 1989; Fuchs et al. 1998) calculates the potentials in nodes at the interfaces of homogeneous isotropically conducting compartments. In general, three compartments are distinguished: the brain which is enclosed by the skull, which is enclosed by the scalp compartment. The geometrical shape of the head is obtained from segmented magnetic resonance images. After preprocessing, the BEM is able to solve the forward problem with one matrix multiplication, which makes it an attractive method to solve the inverse problem.

In reality, several tissues with different conductivities are generally located in the same BEM compartment. To in-

* Department of Electronics and Information Systems, Ghent University, Belgium.

+ Epilepsy Monitoring Unit, Department of Neurology, Ghent University Hospital, Belgium,

Accepted for publication: August 5, 2001.

Bart Vanrumste and Paul Boon are supported by grants from the Fund for Research of the Ghent University, Belgium (Bijzonder Onderzoeksfonds RUG, 01104495 - 011A0996 - 01105399 - 011D0996). Rik Van de Walle is a post-doctoral Fellow of the Fund for Scientific Research Flanders, Belgium. The authors would like to thank Peter Van Hese for his suggestions and clarifying comments.

Correspondence and reprint requests should be addressed to Bart Vanrumste, Department of Electronics and Information Systems, Ghent University, Sint-Pietersnieuwstraat 41, B-9000 Ghent, Belgium.

Fax: +32-9-2404971,

E-mail: bart.vanrumste@elis.rug.ac.be

corporate larger sets of tissues with different conductivities, methods such as the finite element (FEM) (Yan et al. 1991; Awada et al. 1997; Buchner et al. 1997; Weinstein et al. 2000) and finite difference method (FDM) (Witwer et al. 1972; Marino et al. 1993; Laarne et al. 1995; Lemieux et al. 1996; Saleheen and Ng 1997; Vanrumste et al. 1998; Laarne et al. 2000a; Laarne et al. 2000b; Vanrumste et al. 2000) need to be used. In FDM, which is the method used in this paper, the conducting volume is discretized on a cubic grid. In principle, every cubic element can have a different conductivity. The potential value at the center of each element or node can be written as a linear combination of the potentials of six adjacent nodes, as we will see later. Due to the large number of cubic elements, direct solvers for linear systems, such as Gaussian elimination (Datta 1995), cannot be used to obtain the potentials in the nodes. Iterative solvers for large sparse systems of linear equations (Datta 1995) need to be utilized to obtain these potentials for a given source.

For each new dipole the iterative solver must be reapplied. This procedure is rather time consuming when solving the inverse problem. We utilize the finite difference reciprocity method (FDRM) which is able to incorporate multiple inhomogeneities utilizing the FDM, and which is able to perform inverse calculations with a limited number of numerical calculations, by using the reciprocity theorem. The number of numerical calculations will be limited by the number of scalp electrodes considered and not by the number of forward evaluations needed in the inverse procedure. In the past, authors have used the reciprocity theorem in combination with FEM and FDM (Vanrumste et al. 1998; Weinstein et al. 2000; Laarne et al. 2000a; Laarne et al. 2000b; Vanrumste et al. 2000). In the discussion section, we will compare the results found in these publications with our results.

The aim of this paper is to evaluate the performance of FDRM in solving the inverse problem in the three-shell spherical head model, for a large number of test dipoles. The exact electrode potentials are calculated by utilizing the analytical expression, which exists for the forward problem in this geometry. These potentials are then used to investigate the dipole location and orientation error resulting from utilizing the FDRM, with a 2 mm and a 3 mm grid, in the inverse procedure. We also studied the impact of increasing the number of scalp electrodes from 27 to 44 on the performance of the FDRM in solving the inverse problem. We have also compared the sensitivity to noise using FDRM in EEG dipole source analysis with the sensitivity to noise using the analytical expression for the forward problem. It is not our aim to investigate the dipole location error due to noise as such. We only want to compare the sensitivity to noise of FDRM with the one of the analytical method.

Notice that we restricted our investigations to dipole localization errors due to applying the FDRM. There are also other contributors to dipole localization errors, such as noise (Mosher et al. 1993). Moreover, the applied volume conductor model deviates from the real human head. This also leads to dipole localization errors (Awada et al. 1998; Vanrumste et al. 2000). However, these two cases are not discussed in this paper.

The finite difference method

Poisson's differential equation governs the bioelectricity problem:

$$\nabla \cdot (\sigma(\mathbf{r}) \nabla V(\mathbf{r})) = -I\delta(\mathbf{r} - \mathbf{r_2}) + I\delta(\mathbf{r} - \mathbf{r_1}) \qquad (1)$$

where V is the potential and σ is the conductivity tensor at a point $\mathbf{r}$. The right hand side of equation 1 represents the point current source and sink providing I and $-I$ Ampère resp., at positions $\mathbf{r_1}$ and $\mathbf{r_2}$ where $\delta(\mathbf{r} - \mathbf{r}_*)$ denotes the (3-D) delta function centered at $\mathbf{r}_*$. For anisotropic conductivities, the finite difference approximation of equation 1 can be found in Saleheen and Ng (1997). In what follows only isotropic conductivities are considered. The conductivity tensor then becomes a scalar σ. The head model is divided into isotropic piecewise homogeneous compartments. The following boundary conditions hold in a point $\mathbf{r}_0$ at the interface of a compartment A with conductivity σ_A and B with conductivity σ_B:

$$\begin{aligned} \sigma_A \nabla V \cdot \mathbf{n} \Big|_{\substack{\mathbf{r} \to \mathbf{r_0} \\ \mathbf{r} \in A}} &= \sigma_B \nabla V \cdot \mathbf{n} \Big|_{\substack{\mathbf{r} \to \mathbf{r_0} \\ \mathbf{r} \in B}} \\ V(\mathbf{r}) \Big|_{\substack{\mathbf{r} \to \mathbf{r_0} \\ \mathbf{r} \in A}} &= V(\mathbf{r}) \Big|_{\substack{\mathbf{r} \to \mathbf{r_0} \\ \mathbf{r} \in B}} \end{aligned} \qquad (2)$$

with $\mathbf{n}$ a unity vector normal to the interface at $\mathbf{r}_0$. On the scalp-air boundary the homogeneous Neumann condition holds,

$$\sigma_{scalp} \nabla V \cdot \mathbf{n} \Big|_{\substack{\mathbf{r} \to \mathbf{r_0} \\ \mathbf{r} \in scalp}} = 0 \qquad (3)$$

Consider a typical node Q_0 in a cubic grid with internode spacing h. The six neighboring nodes are Q_i (i=1,...,6). For our convenience we assume that the coordinates for Q_0 are (0,0,0) and for Q_i (i=1,...,6) (h,0,0), (-h,0,0), (0,h,0), (0,-h,0), (0,0,h), and (0,0,-h), respectively. We define the cube G_i centered around Q_i with edge h (see figure 1). For each cube G_i a conductivity σ_i is allocated. The differential equation 1 applied to G_0 with boundary conditions (equations 2 and 3) is transformed into a linear equation utilizing the "box integration" scheme (Mitchell and Griffiths 1980). We obtain,

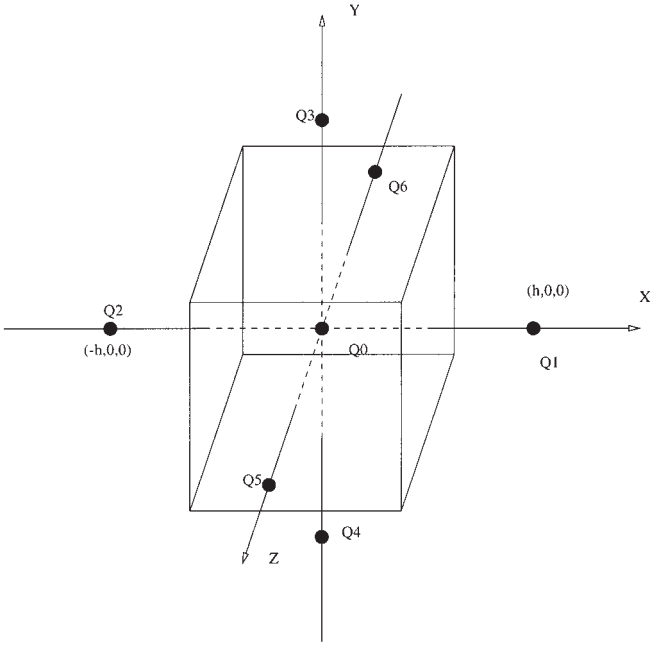

Figure 1. A typical node Q_0 with its neighbors Q_i (i=1...6). The volume G_0 is given by the box.

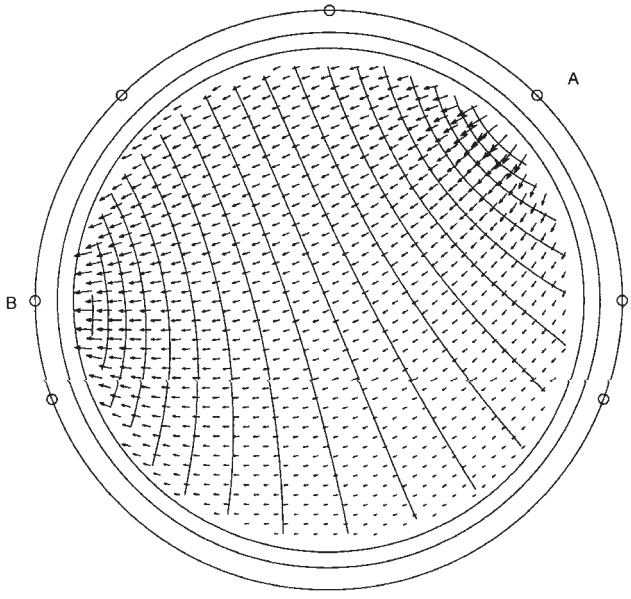

Figure 2. The current density $\mathbf{J}=\sigma\nabla V$ and the equipotential lines in the brain compartment are illustrated when introducing a current I_{AB} at electrode A and removing the same amount at electrode B.

$$\sum_{i=1}^{6}\alpha_i V_{Q_i} - \alpha_0 V_{Q_0} = I_{Q_0} \tag{4}$$

with

$$I_{Q_0} = \iiint_{G_0}\begin{pmatrix} -I\delta(x-x_2)\delta(y-y_2)\delta(z-z_2) \\ +I\delta(x-x_1)\delta(y-y_1)\delta(z-z_1)\end{pmatrix} dx\,dy\,dz$$

and

$$\alpha_i = 2h\frac{\sigma_0\sigma_i}{\sigma_0+\sigma_i}$$

$$\alpha_0 = \sum_{i=1}^{6}\alpha_i$$

For a volume G_0 which contains a current monopole, I_{Q_0} becomes I or $-I$. α_i has the dimension of Ω^{-1} and corresponds with the conductance between Q_0 and Q_i. Furthermore for $I_{Q_0}=0$ we obtain Kirchoff's law at the node Q_0.

For each of the n nodes of the discretized volume model, we obtain a linear equation given by equation 4. As a result, a system of linear equations $\mathbf{SV}=\mathbf{I}$ is obtained. Each of the rows of the system matrix $\mathbf{S}\in\mathbf{IR}^{n\times n}$ contains at most six non-zero off-diagonal elements corresponding with the conductance between the central node and its six neighboring nodes. $\mathbf{V}\in\mathbf{IR}^{n\times 1}$ contains the unknown potentials and $\mathbf{I}\in\mathbf{IR}^{n\times 1}$ corresponds with the current monopoles. We utilize successive overrelaxation (SOR) (Press et al. 1995), an iterative solver of large sparse systems of equations, to obtain the potential distribution at the nodes for a given source configuration. Supposing that $\mathbf{V}^t\in\mathbf{IR}^{n\times 1}$ contains the potentials at the nodes after t iterations, the iterations are stopped when the residual $r^t=|\mathbf{SV}^t-\mathbf{I}|$ does not further decrease.

Reciprocity theorem

In EEG dipole source analysis a large number of forward evaluations need to be performed before the optimal dipole parameters are found. It would be too demanding to calculate for each dipole a forward problem with an iterative solver. Therefore, the reciprocity theorem is utilized in our advantage to reduce the number of forward calculations performed with an iterative solver. To obtain the potential difference U_{AB}, between electrode A and B, for a dipole at position $\mathbf{r}\in\mathbf{IR}^{3\times 1}$ and with components $\mathbf{d}=\left(d_x,d_y,d_z\right)^T\in\mathbf{IR}^{3\times 1}$ with ^{T} the transpose operator, the following steps are considered. A current I_{AB} is introduced at electrode A and removed at electrode B. Utilizing the FDM we then calculate the potentials $V(h.i,h.j,h.k)$ with h the internode spacing and i,j,k the node numbers along the Cartesian axes. Figure 2 illustrates the equipotential lines and current density vectors $\mathbf{J}=\sigma\nabla V$ in the brain compartment with $\nabla V=(\partial V/\partial x,$

$\partial V/\partial y, \partial V/\partial z)^T$. The partial derivative $\partial V/\partial x$ is approximated by $[V(h(i+1),hj,hk)-V(h(i-1),hj,hk)]/2h$. The partial derivatives $\partial V/\partial y$, $\partial V/\partial z$ are obtained in a similar way.

The reciprocity theorem states (Malmivuo and Plonsey 1995),

$$U_{AB} = \frac{\mathbf{d}^T \cdot \nabla V(\mathbf{r})}{I_{AB}} \tag{5}$$

with U_{AB} the potential difference between the scalp electrodes A and B generated by the dipole at position $\mathbf{r}$ and orientation $\mathbf{d}$.

When $\mathbf{r}$ does not coincide with a node, then $\nabla V(\mathbf{r})$ is obtained with tri-linear interpolation (Press et al. 1995). By calculating only one forward problem numerically utilizing SOR, with introducing current monopoles at electrodes A and B, and storing the obtained node potentials in a file, we can obtain U_{AB} for every dipole position and orientation.

When l scalp electrodes are used to measure the EEG then l-1 electrode pairs can be found with linear independent potential differences. Therefore l-1 numerical forward calculations are performed and stored in files. For further processing the l-1 potential differences at the l-1 electrode pairs are transformed in l average referenced potentials at the l electrodes.

The inverse calculation

We have solved the inverse problem by adjusting the dipole parameters until the simulated potentials correspond best with the measured EEG.

The EEG measured by l electrodes at a single time instant can be represented by $\mathbf{U}_{in} \in \mathbf{IR}^{l\times 1}$. The three location parameters and the three components of the dipole are obtained by finding the global minimum of the relative residual energy (RRE):

$$RRE = \frac{\left\|\mathbf{U}_{in} - \mathbf{U}_{model}\right\|^2}{\left\|\mathbf{U}_{in}\right\|^2}$$

with $\mathbf{U}_{model} \in \mathbf{IR}^{l\times 1}$ the electrode potentials obtained by the forward evaluation in the inverse problem. The RRE indicates the fraction of energy which cannot by modeled by the dipole. The solution of the inverse problem can be found by iteratively adjusting the six dipole parameters until a global minimum of RRE is found. However the total number of parameters that have to be optimized can be reduced from six to three. The potential values $\mathbf{U}_{model}$ depend linearly on each of the dipole components $\mathbf{d}=(d_x,d_y,d_z)^T \in \mathbf{IR}^{3\times 1}$. Therefore, the relationship between the dipole components $\mathbf{d}$ and the potential values $\mathbf{U}_{model}$ can be described by a matrix operator $\mathbf{L} \in \mathbf{IR}^{l\times 3}$, the so-called lead field matrix that depends on the dipole position $\mathbf{r}$ but also on the electrode positions, the head geometry and the conductivity profile: $\mathbf{U}_{model} = \mathbf{L}(\mathbf{r}) \cdot \mathbf{d}$, where in $\mathbf{L}$ the first, second and third column consists of the electrode potentials of a unity dipole at position $\mathbf{r}$ with orientation along the x-, y- and z-axis. For a given dipole position $\mathbf{r}$, the optimal components $\mathbf{d}_{opt}$ are found in the least-squares sense (Datta 1995) as the solution of the over determined system of linear equations $\mathbf{U}_{in} = \mathbf{L}(\mathbf{r}) \cdot \mathbf{d}$:

$$\mathbf{d}_{opt} = \mathbf{L}^+ \cdot \mathbf{U}_{in} \text{ with } \mathbf{L}^+ = \left(\mathbf{L}^T\mathbf{L}\right)^{-1}\mathbf{L}^T$$

where $\mathbf{L}^+$ denotes the Moore-Penrose pseudo-inverse of the lead-field matrix $\mathbf{L}$ and ^{T} denotes the transpose operator. The relative residual energy becomes,

$$RRE = \frac{\left\|\mathbf{U}_{in} - \mathbf{L}\cdot\mathbf{d}_{opt}\right\|^2}{\left\|\mathbf{U}_{in}\right\|^2} = \frac{\left\|\left(\mathbf{E}_l - \mathbf{L}\mathbf{L}^+\right)\cdot\mathbf{U}_{in}\right\|^2}{\left\|\mathbf{U}_{in}\right\|^2} \tag{6}$$

where $\mathbf{E}_l \in \mathbf{IR}^{l\times l}$ represents the unity matrix. The relative residual energy is only dependent on the dipole position $\mathbf{r}$. The Nelder-Mead simplex method (Press et al. 1995) is used to find the position $\mathbf{r}_{opt}$ which minimizes equation 6.

Methods

The dipole location and orientation error due to utilizing the FDRM

The performance of the dipole fit with the FDRM in a three-shell spherical head model is evaluated. The radii for the outer boundaries of brain, skull and scalp in the three-shell spherical head model are 80, 85, and 92 mm, respectively. The conductivity of the brain and scalp compartment is typically set 80 times larger than the conductivity of the skull compartment. An analytical expression exists which generates the exact potentials at the electrodes for a given dipole in the brain compartment (Salu et al. 1990).

The 10-20 international electrode placement (Jasper 1958) is used with additionally on each side 3 inferior temporal electrodes which adds to 27 electrodes illustrated as "*" in figure 3. This electrode placement is used in our long-term epilepsy-monitoring unit and is chosen for that reason. To have a higher spatial sampling of the potentials at the scalp surface, 17 extra electrodes are placed, illustrated as "o" in figure 3, adding up to 44 electrodes. In the light of patient comfort in long-term monitoring, 17 extra electrodes are still acceptable.

The x-axis is oriented from the center to the right ear, the y-axis is oriented from the center to the nose, and the

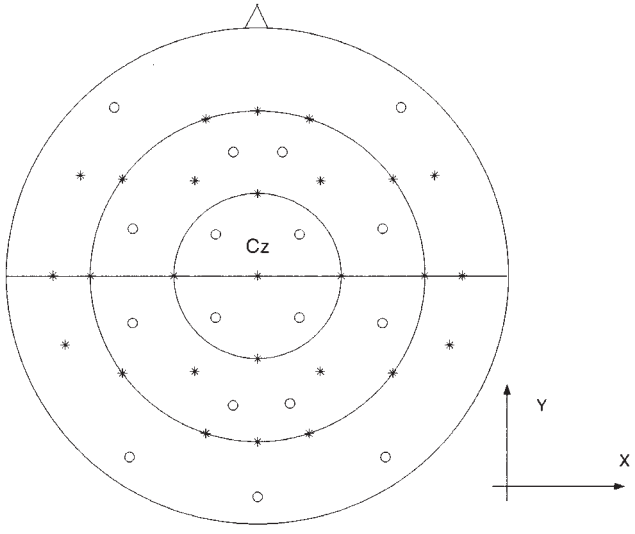

Figure 3. A top view of the electrode positions is given. The large circles represent positions with a constant azimuthal angle θ. From the inner to the outer circle we have a θ of 45°, 90° and 120°, respectively. The 27 electrodes "*" and the additional 17 electrodes "o" are also illustrated. The coordinate axes are also depicted.

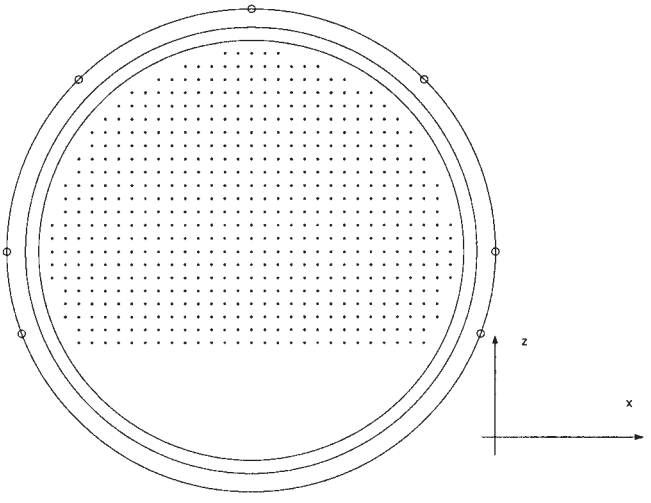

Figure 4. The dipole test positions, illustrated with dots, are located on the coronal slices containing the vertex electrode "Cz".

z-axis (not illustrated) is oriented from the center to the vertex electrode "Cz". We have chosen the node located closest to the central point of the electrode as the electrode node in the discretized volume conductor models.

The test dipoles are placed in the brain compartment as illustrated in figure 4 on the coronal slice containing the vertex electrode "Cz". For each test dipole position three dipoles are generated with dipole orientation along the *x*-, *y*- and *z*-axis. For a total of 1743 dipoles the location and orientation error is investigated for a given FDRM configuration. The dipole location error is the distance between the original and the fitted dipole. The dipole orientation error is the angle between the orientation of the original and the fitted dipole. Four volume conductor model (VCM) configurations are considered. The first configuration consists of a discretized volume conductor model with 2 mm node spacing and 44 scalp electrodes (VCM-2mm-44el), the second configuration consists of a 2 mm grid with 27 electrodes (VCM-2mm-27el), the third configuration consists of a 3 mm grid with 44 electrodes (VCM-3mm-44el), and the fourth configuration consists of a 3 mm grid with 27 electrodes (VCM-2mm-27el).

The choice of the 2 mm and 3 mm grid is based on results found in the literature and on practical considerations. It was found (Laarne et al. 1995) that a 2 mm cubic grid yields potentials which are in good agreement with the ones found applying the analytical expression. Furthermore, realistic volume conductor models are obtained from segmented 3D MR images which have, in our application, cubic voxels with an edge of 1 mm. It is then also convenient to generate cubic grids having an edge which is a multiple of this voxel edge. A 1 mm grid is still too computationally demanding and a 4 mm grid or larger grids cause dipole location errors which are too large.

The sensitivity to noise

The signal-to-noise ratio (SNR) is defined as the root-mean-square of the average referenced potential generated by a dipole, divided by *N*. The noise values have a Gaussian distribution with standard deviation *N* and zero mean.

The SNR of an epileptic spike typically is 5. Aligning the peak activity of the spike and averaging the corresponding potential increases the SNR. The SNR of an averaged spike typically is 10. The SNRs of 5, 10 and 20 are used in the simulations.

We add noise to each of the electrode potentials obtained from the analytical expression. For each test position of the dipole we have generated 400 sets of scalp potentials with added noise. Each distribution is subjected to a dipole fit yielding one fitted dipole position. The inverse problem is solved with FDRM. If we define the location error as the distance between the original and the fitted dipole, we mix 2 types of errors: at the one hand the location error induced by the use of FDRM in the inverse procedure, studied in the noise-free case, and on the other hand the error due to the noise itself. To eliminate the first, we define the location error due to noise as the distance be-

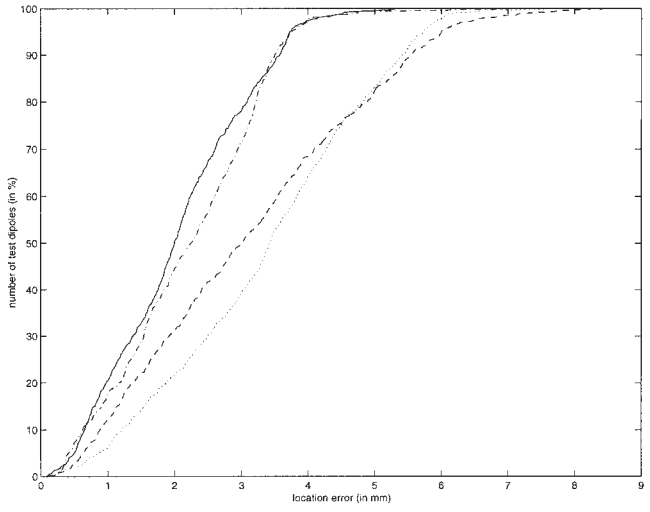

Figure 5. The cumulative distribution of the location error is given when utilizing VCM-2mm-44el(—-), VCM-2mm-27el (·—-·), VCM-3mm-44el (—- —-), and VCM-3mm-27el (···).

tween the dipole position obtained from a dipole fit without noise and the position obtained from a fit with noise. The inverse problem is also solved with the classical method utilizing the analytical expression. This gives us a reference to which FDRM can be compared. The average location error for the 400 sets of noisy potentials are calculated, utilizing VCM-2mm-27el and VCM-3mm-27el, and compared with the average location error found for the case where the inverse problem is solved utilizing the analytical expression and 27 electrodes. We have evaluated the average location error due to noise for two initial dipole positions: one located in the center of the spheres and one located at 50 mm along the vertical axes, both with an orientation along the vertical axes.

The Gaussian noise is uncorrelated between the electrodes, thus is spatially white. In reality background EEG is spatially correlated. For the same SNR this may result in larger dipole location errors. This would be the case when applying FDRM and when applying the analytical expression as forward evaluations in the inverse procedure. It is not expected that one of the methods would suffer more by applying background EEG instead of Gaussian noise. Therefore it is expected that both types of noise can be used to validate the sensitivity to noise of the FDRM.

Results

Calculation time and memory requirements

From empirical tests, we have found that the overrelaxation parameter used in SOR with values ω=1.93 and ω =1.95 yields in general the smallest number of iterations for a 3 mm and a 2 mm grid, respectively. The residual in the SOR method does not further decrease, typically for a 3 mm and a 2 mm grid after about 400 and 500 updates, respectively, utilizing the optimal overrelaxation parameter. The CPU-times needed then for the 3 mm and 2 mm grid is 30 sec and 4 min, respectively, on a Sun Ultra60 workstation with a 300 MHz processor. This brings the total calculation time for 26 and 43 forward calculations, corresponding with 27 and 44 electrodes, and for a 3 mm grid to 13 min and 21 min 30 sec, respectively, and for a 2 mm grid to 1 h 44 min and 2 h 52 min, respectively. A further reduction of the calculation time could be obtained if a more advanced solver would be used such as multigrid solvers (Hoekema et al. 1998).

The number of nodes used for the 3 mm and 2 mm grid equals to 110,483 and 372,189, respectively. The size of the files in which the potential distributions are stored with double precision, for a grid with internode spacing of 3 mm and 2 mm are then, 883,864 bytes and 2,977,512 bytes, respectively. The total sizes for the files containing the node potential of the 26 and 43 forward calculations, and for a 3 mm grid are 22 Mb and 36 Mb, respectively, and for a 2 mm grid are 74 Mb and 122 Mb, respectively.

The location and orientation errors due to the FDRM

Figure 5 illustrates the cumulative distribution of the location error when utilizing VCM-2mm-44el(—), VCM-2mm-27el(—·), VCM-3mm-44el(— —), and VCM-3mm-27el(···). For example, 60% of all the test dipoles have a location error smaller than 2.2 mm, 2.5 mm, 3.5 mm and 3.8 mm for VCM-2mm-44el, VCM-2mm-27el, VCM-3mm-44el and VCM-3mm-27el, respectively. It can also be appreciated that the location error due to utilizing the FDRM is in general smaller than twice the internode spacing of the grid, hence 4 mm for a 2 mm grid and 6 mm for a 3 mm grid, and this independent of the number of electrodes, i.e., 27 or 44. The spatial distribution of the dipole location error is given in figure 6. The gray scale indicates the distance in mm between the original and the fitted dipole. The first, second, and third column presents the dipole location error for dipoles oriented along the *x*-, *y*- and *z*-axis, respectively. Row one, two, three and four in figure 6 present the dipole location errors due to utilizing configurations VCM-2mm-44el, VCM-2mm-27el, VCM-3mm-44el and VCM-3mm-27el, respectively.

We can observe by comparing VCM-2mm-44el and VCM-3mm-44el, that for the same test dipole positions, the dipole location error is obviously smaller utilizing 2 mm grid than a 3 mm grid. The same observation is made when comparing VCM-2mm-27el and VCM-3mm-27el in figure 6.

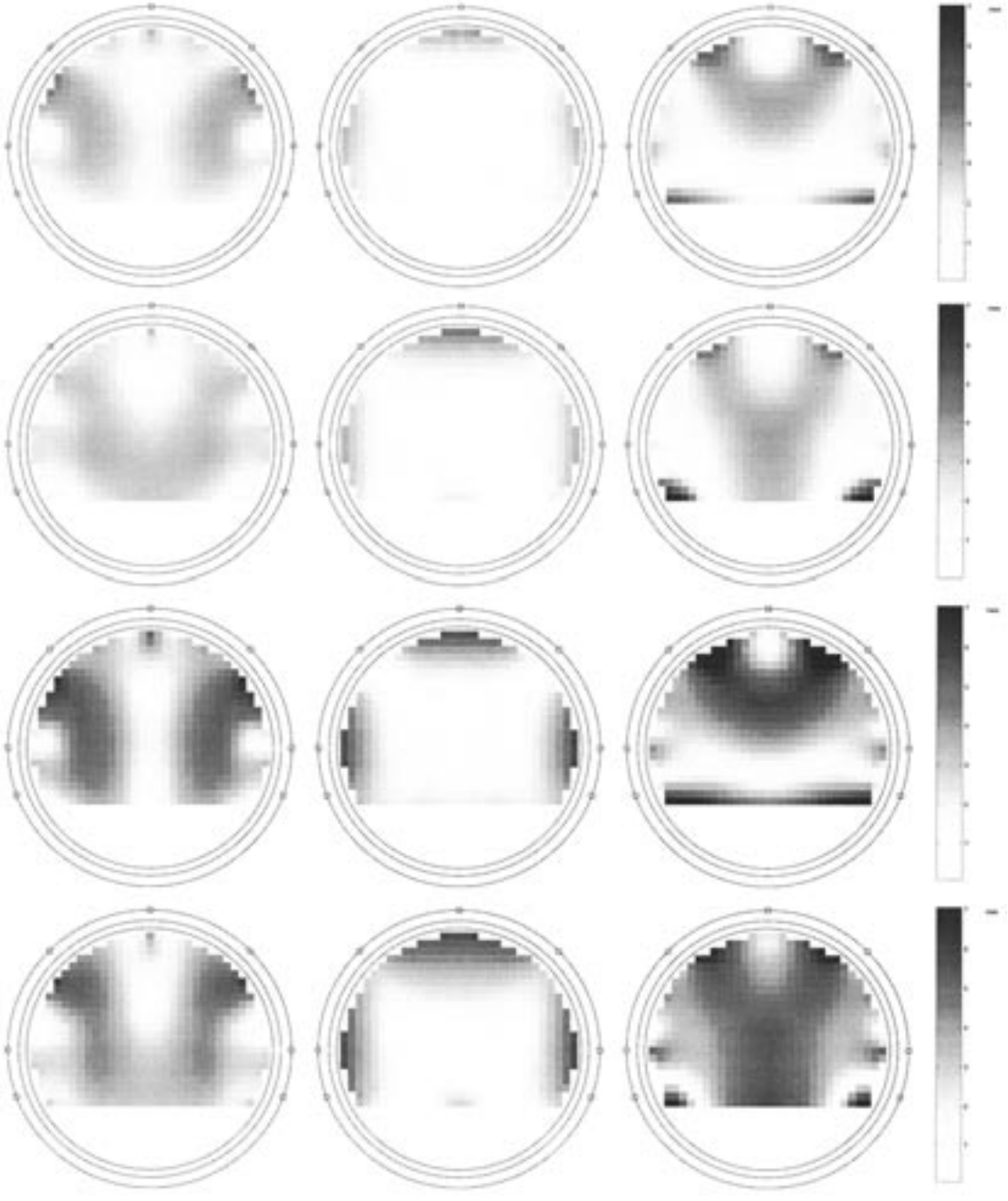

Figure 6. The spatial distribution of the dipole location error is given. The gray scale indicates the distance in mm between the original and the fitted dipole. The first, second, and third column presents the dipole location error for dipoles oriented along the x-, y- and z-axis, respectively. Rows one, two, three, and four present the dipole location errors due to utilizing configurations VCM-2mm-44el, VCM-2mm-27el, VCM-3mm-44el and VCM-3mm-27el, respectively.

We can further notice by comparing VCM-2mm-44el and VCM-2mm-27el that the distribution of the location error does not coincide completely when utilizing an extended set of scalp electrodes. The same result is found when comparing VCM-3mm-44el and VCM-3mm-27el.

In figure 7 the cumulative distribution of the dipole orientation error is illustrated for the four configurations considered. From the figure we can conclude that the dipole orientation error is always smaller than 4°.

The sensitivity to noise

Table I gives the average location error due to noise for a dipole positioned in the center and at an eccentricity of 50 mm along the *z*-axis, both with an orientation along

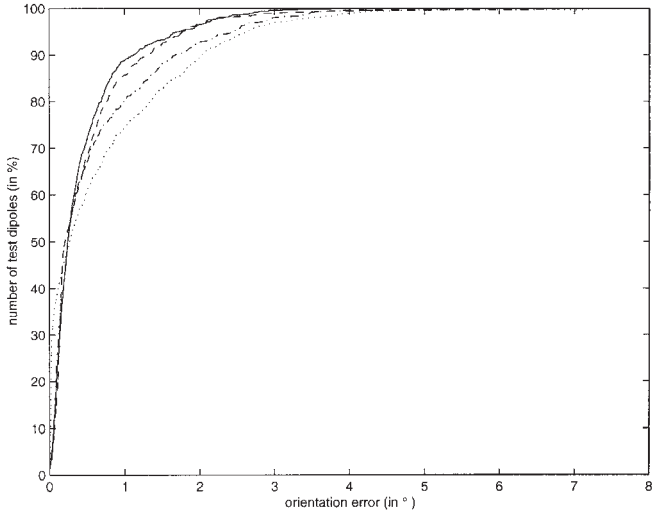

Figure 7. The cumulative distribution of the orientation error is given when utilizing VCM-2mm-44el (—), VCM-2mm-27el (·—·), VCM-3mm-44el (— —), and VCM-3mm-27el (···).

the z-axis. A SNR of 5, 10 and 20 is used. $|\Delta r_{3mm-27el}|$ and $|\Delta r_{2mm-27el}|$ are the distance between the fitted dipole position in the noiseless case and the fitted dipole position in the noisy case for the configurations VCM-3mm-27el and VCM-2mm-27el, respectively. $|\Delta r_{ana-27el}|$ is the distance between the original dipole position and the fitted dipole position in the noisy case applying the analytical expression. By inspecting the rows of table I we can appreciate that the average location errors by using the VCM-2mm-27 and VCM-3mm-27 are similar to the location errors utilizing the analytical expression. Hence this indicates that the sensitivity to noise when utilizing the FDRM is of the same order as the one found utilizing the analytical expression.

In figure 8 the dots present the dipole fits from the distributions with added noise for a dipole located at position (0,0,0) and (0,0,50) mm and orientation along the z-axis. The location error can be inspected for the x- and z-coordinate. The y-coordinate is projected on the coronal slice. In figure 8 a SNR = 10 is used. The "+" indicates the original dipole position and the "×" indicates the fitted dipole position without noise. We can appreciate from figure 8 that the cloud of dots is more concentrated in the vicinity of "×" rather than of "+".

Discussion

The position errors observed in the noise-free case are only due to nonzero grid spacing. For example, we have chosen the node of the structured grid which is closest to the electrode position as the electrode node. Usually the electrode position and the electrode node do not coincide. Subsequently this contributes to the dipole position errors. The left-right symmetry of the position errors in figure 6 is due to the left-right symmetric electrode distribution and the left-right symmetry of the computational grid.

A potential disadvantage is that the method, for now, is rather slow compared with the BEM. However by applying faster solvers, such as the multigrid solvers, the calculations can be sped up.

Next, we compare the results found in our study with the ones found in the literature. The forward evaluation of reciprocity in combination with the FDM for EEG was first investigated in (Laarne et al. 1995). This paper evaluated the forward problem applying the FDRM. The potentials were calculated in the volume conductor model for a current source and sink, diametrically placed on the surface of a three-shell spherical head model. These potentials were compared with the ones found uti-

Table I. Average location error due to noise utilizing VCM-3mm-27, VCM-2mm-27, and the analytical expression in the inverse problem, for dipoles positioned on the z-axis with eccentricity of 0 mm and 50 mm, respectively. Both test dipoles have an orientation along the z-axis. The SNR values are 5, 10 and 20.

Dipole position	**SNR**	**VCM-3mm-27el**	**VCM-2mm-27el**	**analytical**
On z-axis (mm)		$E(\lvert\Delta r_{3mm-27el}\rvert)$ (mm)	$E(\lvert\Delta r_{2mm-27el}\rvert)$ (mm)	$E(\lvert\Delta r_{ana-27el}\rvert)$ (mm)
0	5	6.1	6.1	6.2
	10	2.9	3.0	3.1
	20	1.5	1.5	1.6
50	5	4.7	4.7	4.7
	10	2.3	2.3	2.3
	20	1.2	1.1	1.2

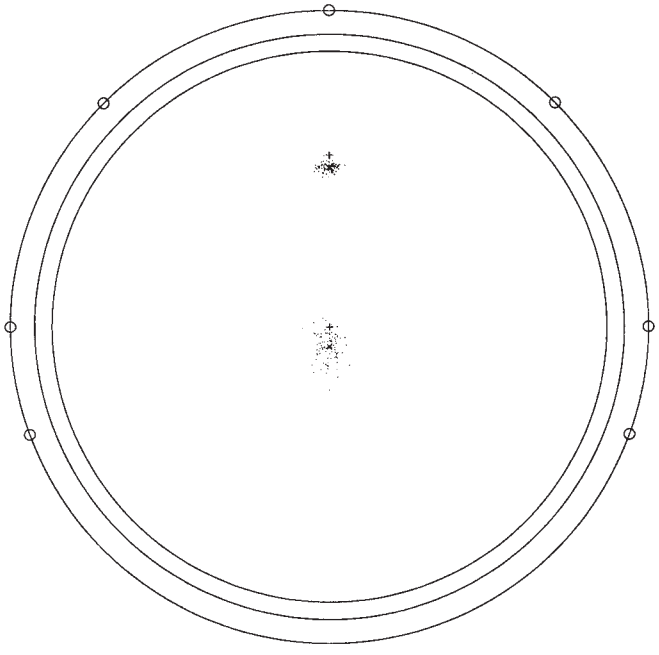

Figure 8. The dots represent solutions of the inverse problem from potentials added with noise. The "+" indicates the original dipole position while the "x" represents the fitted position without noise. A SNR=10 is depicted.

lizing the analytical expression. It was found that a 2 mm cubic grid yields potentials which are in good agreement with the ones found applying the analytical expression.

Furthermore the same group (Laarne et al. 2000b) reported the inverse problem calculated for 45 test dipoles in a 2 mm cubic grid. They solved the forward problem with the FDM in a realistic head model, using a dipole source. Then they used the FDRM in the forward evaluations of the inverse procedure to retrieve the original test dipole. The average position error was 2.8 mm, when applying 19 electrodes and 2 mm for 58 electrodes. The orientation errors were on average 8° and 6.5° for 19 and 58 electrodes, respectively. These results are in agreement with our results. However, one can argue that the potentials calculated in the forward problem were already exposed to errors due to the utilization of the FDM. Subsequently it is difficult to evaluate whether the dipole position errors are due to the errors in the inverse procedure or due to errors in the forward problem.

Reciprocity in combination with the FEM, was introduced in Weinstein et al. (2000). They calculated the potentials at the scalp with the FEM and with a dipole source. Then they applied the FEM in combination with the reciprocity theorem to calculate the optimal dipole at each element of the FEM grid. The dipole with the lowest residual energy was found close to the original source. We are not aware of a more systematic validation of reciprocity in combination with the FEM.

Finally, the results found for a state of the art BEM (Leahy et al. 1998) are compared with the results found in our study. A part of their study dealt with the validation of the BEM in a three-shell spherical head model. Each shell was tessellated by 2292 triangles, with a side of about 6-8 mm. Thirty-two test dipoles were placed in different areas of the brain. Furthermore, three electrode sets were applied: 65 electrodes, mainly placed at the left back portion of the scalp, 61 electrodes more homogeneously spread over the scalp surface and a dense grid of 148 electrodes. The average position error for these three electrode sets were, 1.78 mm, 2.04 mm and 1.77 mm, respectively. These values are of the same order as the values found in our simulation for a 2 mm grid. More specifically, we found average position errors of 2.2 mm and 2.0 mm for 27 and 44 electrodes, respectively.

Conclusions

The FDM provides the opportunity to easily incorporate tissue with a specific conductivity (such as the ventricular system, white and gray matter, bore holes in the skull, air cavities, etc.) in the head model. The reciprocity theorem provides the ability to reduce the number of iteratively solved potential distributions to the number of electrode pairs considered. This gives a substantial reduction of calculation time compared with the procedure in which for each forward evaluation in the inverse problem, an iteratively solved potential distribution needs to be calculated. The performance of FDRM in EEG dipole source localization is investigated in the analytically solvable three-shell spherical head model for 1745 test dipoles. We have found that the location error is in general not larger than twice the internode distance and this independent of the number (27 or 44) of electrodes used. The orientation error is always smaller than 4° for all the test dipoles and all the FDRM configurations considered. We have also compared the sensitivity to noise using FDRM in the inverse problem of EEG dipole source analysis with the sensitivity to noise using the analytical expression. We have found that FDRM is not more sensitive to noise than the method using the analytical expression.

References

Awada, K.A., Jackson, D.R., Baumann, S.B., Williams, J.T., Wilton, D.R., Fink, P. and Prasky, B. Effects of conductivity uncertainties and modeling errors on EEG source localization using a 2-D model. IEEE Transactions on Biomedical Engineering, 1998, 45(9): 1135-1145.

Awada, K.A., Jackson, D.R., Williams, J.T., Wilton, D.R., Baumann, S.B. and Papanicolaou, A.C. Computational aspects of finite element modeling in EEG source localiza-

tion. IEEE Transactions on Biomedical Engineering, 1997, 44(8): 736-752.

Boon, P. and D'Havé, M. Interictal and ictal dipole modelling in patients with refractory partial epilepsy. Acta Neurologica Scandinavia, 1995, 92: 7-18.

Boon, P., D'Havé, M., Vonck, K., Baulac, M., Vanderkerckhove, T. and De Reuck, J. Dipole modeling in epilepsy surgery candidates. Epilepsia, 1996, 38(2): 208-218.

Buchner, H., Knoll, G., Fuchs, M., Rienäcker, A., Beckmann, R., Wagner, M., Silny, J. and Pesch, J. Inverse localization of electric dipole current sources in finite element models of the human head. Electroencephalography and Clinical Neurophysiology, 1997, 102(4): 267-278.

Datta, B.N. Numerical Linear Algebra and Applications. Brooks/Cole Publishing Company, 1995.

Ebersole, J.S. and Wade, P.B. Spike voltage topography and equivalent dipole localization in complex partial epilepsy. Brain Topography, 1990, 3(1): 21-34.

Fuchs, M., Drenckhahn, R., Wischmann, H.-A. and Wagner, M. An improved boundary element method for realistic volume-conductor modeling. IEEE Transactions on Biomedical Engineering, 1998, 45(8): 980-997.

Hoekema, R., Venner, K., Struijk, J.J. and Holsheimer, J. Multigrid solution of the potential field in modeling electrical nerve stimulation. Computers and Biomedical Research, 1998, 31: 348-362.

Jasper, H. Report of committee on methods of clinical exam in EEG. Electroencephalography and Clinical Neurophysiology, 1958, 10: 370-375.

Laarne, P.H.E., Hyttinen, J., Suihko, V. and Malmivuo, J. Validation of a detailed computer model for the electric fields in the brain. Journal of Medical Engineering and Technology, 1995, 19(2-3): 84-87.

Laarne, P., Hyttinen, J., Dodel, S., Malmivuo, J. and Eskola, H. Accuracy of two dipolar inverse algorithms applying reciprocity for forward calculation. Computers and Biomedical Research, 2000a, 33(3): 172-185.

Laarne, P., Tenhunen-Eskelinen, M.J.H. and Eskola, H. Effect of EEG electrodes density on dipole localization accuracy using two realistically shaped skull resistivity models. Brain Topography, 2000b, 12(4): 249-254.

Leahy, R.M., Mosher, J.C., Spencer, M.C., Huang, M.X. and Lewine, J.D. A study of dipole localization accuracy for MEG and EEG using a human skull phantom. Electroencephalography and Clinical Neurophysiology, 1998, 107(2): 159-173.

Lemieux, L., McBride, A. and Hand, J.W. Calculation of electrical potentials on the surface of a realistic head model by finite differences. Phys. Med. Biol., 1996, 41: 1079-1091.

Lopes da Silva, F. Event-related potentials: Methodology and quantification. In: E. Niedermeyer and F. Lopes da Silva (Eds.), Electroencephalography, Basic Principles, Clinical Applications and Related Fields. Urban and Schwarzenberg, 1987, 46 (2nd edition): 763-772.

Malmivuo, J. and Plonsey, R. Bioelectromagnetism: Principles and Applications of Bioelectric and Biomagnetic Fields. Oxford University Press, New York, 1995.

Marino, F., Halgren, E., Badier, J.-M., Gee, M. and Nenev, V. A finite difference model of electric field propagation in the human head: Implementation and validation. In: Proceedings of the 19th Annual Northeast Bioengineering Conference, 1993: 82-85.

Meijs, J.W.H., Weier, O.W., Peters, M.J. and Oosterom, A. On the numerical accuracy of the boundary element method. IEEE Transactions on Biomedical Engineering, 1989, 36(10): 1038-1049.

Mitchell, A. and Griffiths, D. The finite difference method in partial differential equations. John Willey and Sons, 1980.

Mosher, J.C., Spencer, M.E., Leahy, R.M. and Lewis, P.S. Error bounds for EEG and MEG dipole source localization. Electroencephalography and Clinical Neurophysiology, 1993, 86: 303-321.

Press, W.H., Teukolsky, S.A., Vetterling, W.T. and Flannery, B.P. Numerical recipes in C. Cambridge University Press, 1995.

Saleheen, H.I. and Ng, K.T. New finite difference formulations for general inhomogeneous anisotropic bioelectric problems. IEEE Transactions on Biomedical Engineering, 1997, 44(9): 800-809.

Salu, Y., Cohen, L.G., Rose, D., Sato, S., Kufta, C. and Hallett, M. An improved method for localizing electric brain dipoles. IEEE Transactions on Biomedical Engineering, 1990, 37(7): 699-705.

Schaul, N. The fundamental neural mechanisms of electroencephalography. Electroencephalography and Clinical Neurophysiology, 1998, 106: 101-107.

Vanrumste, B., Van Hoey, G., Boon, P., D'Havé, M. and Lemahieu, I. Inverse calculations in EEG source analysis applying the finite difference method, reciprocity and lead fields. In: Proceedings of the 20th Annual International Conference of the IEEE Engineering in Medicine and Biology Society, 1998: 2112-2115.

Vanrumste, B., Van Hoey, G., Van de Walle, R., D'Havé, M., Lemahieu, I. and Boon, P. Dipole localization errors in electroencephalogram source analysis due to volume conductor model errors. Med. Biol. Eng. Comput., 2000, 38(5): 528-534.

Weinstein, D., Zhukov, L. and Johnson, C. Lead-field bases for electroencephalography source imaging. Annals of biomedical engineering, 2000, 28: 1059-1065.

Witwer, J.G., Trezek, G.J. and Jewett, D.L. The effect of media inhomogeneities upon intracranial electrical fields. IEEE Transactions on Biomedical Engineering, 1972, BME-19(5): 352-362.

Yan, Y., Nunez, P. and Hart, R. Finite element model of the human head: scalp potentials due to dipole sources. Med. Biol. Eng. Comput., 1991, 29: 475-481.